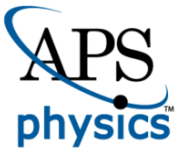

Scalar fields in black hole spacetimes

Izak Thuestad, Gaurav Khanna, and Richard H. Price

Phys. Rev. D **96**, 024020 — Published 14 July 2017

DOI: 10.1103/PhysRevD.96.024020

Scalar Fields in Black Hole Spacetimes

Izak Thuestad and Gaurav Khanna
Department of Physics, University of Massachusetts, Dartmouth, MA 02747

Richard H. Price
Department of Physics, MIT, 77 Massachusetts Ave., Cambridge, MA 02139 and
Department of Physics, University of Massachusetts, Dartmouth, MA 02747

The time-evolution of matter fields in black hole exterior spacetimes is a well-studied subject, spanning several decades of research. However, the behavior of fields in the black hole interior spacetime, has only relatively recently begun receiving some attention from the research community. In this paper, we numerically study the late-time evolution of scalar fields in both Schwarzschild and Kerr spacetimes, including the black hole interior. We recover the expected late-time power-law "tails" on the exterior (null infinity, time-like infinity and the horizon). In the interior region, we find an interesting oscillatory behavior that is characterized by the multipole index ℓ of the scalar field. In addition, we also study the extremal Kerr case and find strong indications of an instability developing at the horizon.

I. INTRODUCTION

Study of fields in black hole (exterior) spacetimes has been a popular area of research over many decades. Such research has often yielded many intriguing aspects of black hole physics. For instance, the notion of quasi-normal ringing as a characteristic feature of such spacetimes recently helped LIGO discover gravitational waves from a binary black hole system [1, 2] for the first time ever.

Another interesting feature of physical fields evolving in black holes spacetimes is their late-time, power-law decay behavior – so-called "tails". This discovery was made by Richard Price nearly half-a-century ago in the context of a Schwarzschild black hole [3]. However, it has continued to be an area of active research in the Kerr black hole context [4, 5] even as recently as the last few years [6].

Naturally, nearly all the focus of research in this area happens to be in the context of the black hole exterior spacetime. However, recently interest in the interior spacetime has also been increasing and a number of intriguing results have emerged [7–11].

In this paper, we study the late-time behavior of scalar fields (to linear order) over the entire black hole spacetime, including the interior region. We consider both Schwarzschild and Kerr black holes for this study. Late-time tail results for the exterior black hole spacetimes are known, and we compare our results with those (horizon, timelike and null infinity) for validation purposes. The main new results we present in this work relate to the late-time behavior of scalar fields in the black hole interior region. In order to perform such a study, we make use of advanced mathematical (hyperboloidal compactification) and computational techniques (high-precision GPU-computing), the details of which appear in the following sections. In this work, we focus on axisymmetric, scalar field configurations. Other, more general cases will be presented elsewhere.

Our work involves using compactified ingoing Kerr coordinates to perform computations that cover the entire interior and exterior black hole spacetime. These coordinates were successfully used in recent work to perform a detailed study of the Cauchy horizon [9] of a rotating black hole. We find that while there is a way to view the late-time decay of the fields in the black hole interior as a power-law tail, an infalling physical detector would actually record a finite number of oscillatory cycles[1] before encountering the spacetime singularity. The number of oscillatory cycles depends on the multipole index of the field, and also whether the black hole is spinning or not.

We also include a short section on the late-time behavior of scalar fields at the horizon of an extremal Kerr black hole, and report on an indication of the formation of an asymptotic instability, as very recently uncovered in the research literature [13, 14].

This paper is organized as follows: Section II offers details on our methodology, i.e. the approach we take in solving the scalar Teukolsky equation using suitable coordinates that allow us to "penetrate" the black hole horizon and continue to evolve the fields into the interior region; Section III documents our numerical results and the comparisons with expectations based on previous work; and finally, we end with a brief summary and statement on future work in Section IV.

II. NUMERICAL SOLUTION OF THE TEUKOLSKY EQUATION

In this section we briefly document the background and computational methods used to generate the results in the upcoming sections of this paper. We provide here a description of the coordinate-systems used, the relevant

[1] These are different from the oscillations on the Cauchy horizon as found by Ori in 1992 [12] in the context of a Kerr black hole.

evolution equations and the computational techniques employed.

The main context of this work is the behavior of scalar fields in the spacetime of a rotating black hole (Kerr), including the special case of a non-rotating (Schwarzschild) hole. The common coordinate system that is used to describe the spacetime of black holes is the Boyer-Lindquist system (t, r, θ, φ) that has close similarities with spherical coordinates. However, Boyer-Lindquist coordinates are not the best suited to study the black hole interior spacetime because they suffer from a coordinate-singularity at the horizon locations. Since we are interested in studying the behavior of fields in the interior region too, we instead make use of a better suited coordinate system, i.e. ingoing Kerr coordinates. These are a Kerr spacetime generalization of the better-known Eddington-Finkelstein coordinates that are able to smoothly "penetrate" the horizon of a Schwarzschild black hole. In the following subsection, we review the relationship between these different coordinate systems and emphasize some of their important aspects.

The main evolution equation of interest in this work is the Teukolsky master equation that describes scalar, vector and tensor field perturbations in the spacetime of a Kerr black hole [15] to linear order. We numerically solve this equation for the scalar field case using a compactified form of the ingoing Kerr coordinates. Using hyperboloidal compactification allows us to *directly* sample the behavior of fields throughout the spacetime, including even null infinity $\mathscr{I}^+$. One important aspect of this work worth noting is that we must evolve the fields for a long duration because we are interested in the late-time, power-law decay behavior of the fields. This behavior typically appears *after* the quasi-normal modes of the system have exponentially decayed enough to become subdominant. This posed certain challenges that are explained in some detail in the following sections.

The following subsections offer additional details including the main expressions for the quantities involved and also our computational methodology.

A. Teukolsky Equation in Ingoing-Kerr Coordinates

We begin with an expression of the usual Boyer-Lindquist coordinate version of the Kerr spacetime metric and the associated Teukolsky equation [15]. The metric has the form

$$\begin{aligned} ds^2 &= (1 - 2Mr/\Sigma)\, dt^2 \\ &+ \left(4Mar\sin^2\theta/\Sigma\right) dt d\varphi - \left(\frac{\Sigma}{\Delta}\right) dr^2 - \Sigma d\theta^2 \\ &- \sin^2\theta \left(r^2 + a^2 + 2Ma^2 r \sin^2\theta/\Sigma\right) d\varphi^2, \end{aligned} \tag{1}$$

where $\Sigma = r^2 + a^2\cos^2\theta$ and $\Delta = r^2 - 2Mr + a^2$. Here M refers to the black hole mass and the Kerr parameter a characterizes the hole's spin. It is clear that the metric exhibits pathological behavior at the horizon locations, i.e. when $\Delta = 0$. Note that this coordinate singularity can be easily removed by a suitable change of coordinates. The Teukolsky master equation takes the form

$$\begin{aligned} &-\left[\frac{(r^2+a^2)^2}{\Delta} - a^2\sin^2\theta\right]\partial_{tt}\Psi - \frac{4Mar}{\Delta}\partial_{t\phi}\Psi \\ &-2s\left[r - \frac{M(r^2-a^2)}{\Delta} + ia\cos\theta\right]\partial_t\Psi \\ &+\Delta^{-s}\partial_r\left(\Delta^{s+1}\partial_r\Psi\right) + \frac{1}{\sin\theta}\partial_\theta\left(\sin\theta\partial_\theta\Psi\right) + \\ &\left[\frac{1}{\sin^2\theta} - \frac{a^2}{\Delta}\right]\partial_{\phi\phi}\Psi + 2s\left[\frac{a(r-M)}{\Delta} + \frac{i\cos\theta}{\sin^2\theta}\right]\partial_\phi\Psi \\ &-\left(s^2\cot^2\theta - s\right)\Psi = 0, \end{aligned} \tag{2}$$

where in addition to the previously defined quantities, s refers to the "spin weight" of the matter field. As remarked before, this evolution equation determines the dynamical behavior of matter fields in the spacetime of a Kerr black hole. The $s = 0$ version of this equation describes the evolution of a scalar field Ψ in a black hole spacetime, which is the case of interest in this work.

To remove the coordinate singularity at the horizon locations, we consider the above equations in a different coordinate system. We summarize below the ingoing Kerr coordinate system $(\tilde{t}, r, \theta, \tilde{\varphi})$ and also the Teukolsky equation in these so-called "horizon penetrating" coordinates. In ingoing Kerr coordinates, the Kerr metric is given by

$$\begin{aligned} ds^2 &= \left(1 - \frac{2Mr}{\Sigma}\right) d\tilde{t}^2 - \left(1 + \frac{2Mr}{\Sigma}\right) dr^2 - \Sigma\, d\theta^2 \\ &- \sin^2\theta\left(r^2 + a^2 + \frac{2Ma^2 r}{\Sigma}\sin^2\theta\right) d\tilde{\varphi}^2 - \frac{4Mr}{\Sigma}\, d\tilde{t}\, dr \\ &+ \frac{4Mra}{\Sigma}\sin^2\theta\, d\tilde{t}\, d\tilde{\varphi} + 2a\sin^2\theta\left(1 + \frac{2Mr}{\Sigma}\right) dr\, d\tilde{\varphi}\,. \end{aligned} \tag{3}$$

These coordinates are related to the Boyer-Lindquist coordinates through the transformations $\tilde{\varphi} = \varphi + \int a\Delta^{-1}\, dr$ and $\tilde{t} = t - r + r_*$, where the "tortoise" radial coordinate $r_* = \int (r^2 + a^2)\Delta^{-1}\, dr$. This system does not suffer from any pathologies at the horizon locations and is therefore well-suited for analyzing fields both in the exterior and interior spacetimes of a rotating black hole.

It is important to point out how the physical meaning of these $(\tilde{t}, r, \theta, \tilde{\varphi})$ coordinates changes as one approaches and crosses the horizon from the exterior region of the black hole spacetime into the interior. To illustrate this, we switch to the Schwarzschild case for simplicity, by setting the Kerr parameter $a = 0$. In that case, the ingoing Kerr coordinates relate to the more familiar Eddington-Finkelstein coordinates via $\tilde{t} = v - r$, and exhibit similar qualitative behavior at the (outer) horizon. In Figure 1 we show the Kruskal diagram of the $\tilde{t}$ = constant slices over the entire exterior and interior regions. It is clear that the slices stay well behaved as they cross the horizon and even stay spacelike throughout. However, this is

not the case for the r = constant slices. The constant-r slices (note that for these slices $ds^2 = \left(1 - \frac{2M}{r}\right) d\tilde{t}^2$ if $d\theta = d\tilde{\varphi} = 0$) are timelike outside the horizon and switch to becoming spacelike in the black hole interior region.

The fact that the constant-r slices are not timelike everywhere poses a challenge in how we interpret the time evolution results of a physical field. Typically, a scalar field's values $\Psi(\tilde{t}, r, \theta, \tilde{\varphi})$ at a fixed $(r, \theta, \tilde{\varphi})$ location would be interpreted as the time-series result of a detector sampling the field at that spatial point. The detector is, of course, a physical object and therefore it must have a timelike worldline through the spacetime. This works just as expected in the exterior region of the black hole spacetime. However, in the black hole interior, clearly the detector cannot be located at a constant value of r because that would translate to a spacelike worldline. Any physical detector must take a timelike path which results in a decrease in its r coordinate value as $\tilde{t}$ advances. Once the $r = 0$ singularity is reached (which occurs in a finite proper time), any physical meaning associated to these mathematical quantities is simply lost. Thus, caution must be taken in interpreting any results from a $\tilde{t}$ evolution in the black hole interior region.

Finally, it is useful to note that at the horizon location at late times, the $\tilde{t}$ variable is essentially the null variable $v = t + r_*$.

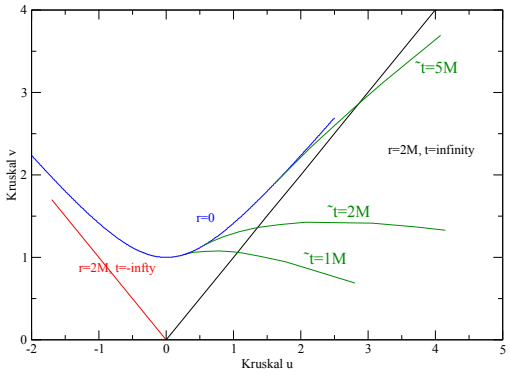

FIG. 1: Constant-$\tilde{t}$ slices of Schwarzschild spacetime plotted on a background of Kruskal coordinates u and v as defined, in terms of Schwarzschild (t, r) coordinates, in Eqs. (31.18), and as pictured in Fig. 31.4(b) of Ref. [16]. The diagonal line on the right is the event horizon at $r = 2M$. The curves plotted show how the constant $\tilde{t}$ slices extend from the black hole interior to exterior regions.

The Teukolsky equation for the scalar field Ψ in these ingoing Kerr coordinates can be derived using a rescaling of the Kinnersley tetrad [17]. It is given by

$$
\begin{aligned}
&(\Sigma + 2Mr)\frac{\partial^2\Psi}{\partial\tilde{t}^2} - \Delta\frac{\partial^2\Psi}{\partial r^2} - 2(r-M)\frac{\partial\Psi}{\partial r} \\
&-\frac{1}{\sin\theta}\frac{\partial}{\partial\theta}\left(\sin\theta\frac{\partial\Psi}{\partial\theta}\right) - \frac{1}{\sin^2\theta}\frac{\partial^2\Psi}{\partial\tilde{\varphi}^2} - 4Mr\frac{\partial^2\Psi}{\partial\tilde{t}\partial r} \\
&-2a\frac{\partial^2\psi}{\partial r\partial\tilde{\varphi}} - 2M\frac{\partial\psi}{\partial\tilde{t}} = 0\,,
\end{aligned}
\tag{4}
$$

and is well-behaved at the horizon locations, and therefore can be used to safely evolve data across it.

The last ingredient that goes into the setup of our coordinate system is hyperboloidal compactification as developed by Zenginoğlu [18]. To do this, we define a compactified coordinate system $(\tau, \rho, \theta, \tilde{\varphi})$ by

$$\tau = \tilde{t} - r^2/(r+S) + 4\ln[S/(r+S)] \tag{5}$$

and

$$\rho = r/[1 + r/S] \tag{6}$$

where a free parameter S controls both the domain and also the foliation. Note that $\rho \in [0, S)$ maps $r \in [0, \infty)$ and is therefore a one-to-one compactifying coordinate. A Penrose diagram of the slices defined by these coordinates in the Kerr spacetime context, adapted from Ref. [9], is presented in Fig. 2. We do not show the final form of the Teukolsky master equation in these compactified coordinates because of the lengthy nature of the expression and the fact that it is not particularly illuminating. We simply refer the reader to the recent relevant research literature [19, 20] wherein additional details may be found.

The computational grid is defined as a uniform grid over the compactified ρ coordinate. As pointed out earlier, this allows us to access null infinity directly on the computational grid ($\rho = S$ maps to $\mathscr{I}^+$). Moreover, the compactification offers a "clean" solution to the so-called "outer boundary problem" in numerical relativity. Typical boundary conditions used in the research community lead to spurious wave reflections from the edge of the computational grid. However, with the approach of hyperboloidal compactification, one is able to extend the computational domain to infinity, making it possible to completely eliminate any such reflections [19]. In addition, the compactification allows us to employ a very dense computational grid (typically, $S \sim 20$) which results in highly accurate numerical results. Those details are provided in the next subsection.

Once again, it is useful to point out that at the horizon locations the τ variable is essentially the same as the null variable v.

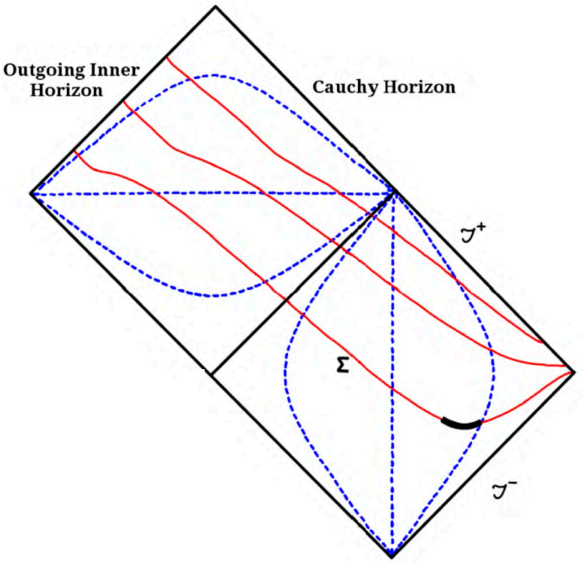

FIG. 2: Penrose diagram of the computational domain for the Kerr spacetime case, adapted from Ref. [9]. The constant ρ (dotted lines) and constant τ (solid lines) slices are clearly marked. In addition, on the initial Cauchy slice Σ we also mark (thick black) where the compactly-supported initial data is non-zero.

B. Computational Methodology

The numerical approach used to solve the Teukolsky equation in the compactified ingoing Kerr coordinate system is very similar to the one presented in our earlier work [19]. We simply outline the main steps here and refer the reader to that reference for additional details. We begin by taking advantage of Kerr spacetime's axisymmetry and separating out the $\tilde{\varphi}$ dependence of the system using an $\exp(im\tilde{\varphi})$ form for the scalar field Ψ. This transforms the original (3+1)D equation into a system of (2+1)D equations. In this work we restrict ourselves to axisymmetric fields only, and therefore we set $m = 0$ throughout. Next, we cast the equations into a first-order hyperbolic partial differential equation form, by defining a new "momentum" field that is related to the derivative of the scalar field Ψ. Finally, we implement a time-explicit, two-step Richtmeyer-Lax-Wendroff, second-order[2] finite-difference evolution scheme[3] This numerical method is stable, and converges to the expected second-order accuracy [19].

It is worth commenting on the fact that numerical computations are rather challenging in the context of studying the late-time tails. As remarked before, these computations must be long duration because the observed field initially exhibits an exponentially decaying oscillatory behavior, i.e. quasi-normal ringing. Only much later, once the exponential decay has made these modes subdominant, does the field transition over to a power-law tail. Moreover, there are often intermediate tails [22], that do not necessarily have the true late-time asymptotic rates that we are interested in here. These intermediate tails decay faster than the asymptotic rate, but may have dominant amplitudes for a period of time. We must evolve longer than these intermediate tails last in order to obtain the tail solution with the true asymptotic decay rate.

In addition, each of the field's spherical harmonic multipoles $Y_{\ell m}$ has its own decay rate (that is proportional to ℓ). Thus, at late times we obtain numerical data in which different multipoles may have widely ranging amplitudes (typically $20-30$ orders of magnitude apart!). It is thus important for the numerical solution to have high grid density in order to reduce the *truncation* errors to very low levels. In addition, due to the very large range of amplitudes involved, these computations also require high-precision floating-point numerics that allow us to reduce *round-off* error that can otherwise easily overwhelm the fast decaying multipoles. In particular, we satisfy this requirement by using *octal*-precision numerics (256-bit or $\sim$60 decimal digits). This keeps the round-off error in our computations at acceptably low levels.

Finally, to complete these long duration, high-accuracy and high-precision computations in a reasonable timeframe we make extensive use GPGPU-based parallel computing. For additional details on implementation of such intensive computations on a parallel GPU architecture, we refer the reader to our earlier work on the subject [23].

III. NUMERICAL RESULTS

In this section, we present the results generated from the numerical solution of the scalar Teukolsky equation in compactified, ingoing Kerr coordinates. As outlined in the previous sections, our approach allows us to evolve data through the horizon and we are thus able to study the late-time behavior of physical fields in both the black hole exterior and interior regions. Our emphasis in this work is the late-time, power-law tails behavior of different spherical harmonic multipoles $Y_{\ell m}$ of a scalar field in both Schwarzschild and Kerr black hole spacetimes. In addition, we restrict ourselves to the axisymmetric case only in this work.

The computational domain is set up as follows: For the Kerr cases, the inner boundary with a Neumann boundary condition is located at the inner horizon, while the

[2] In fact, the angular differentiation (the θ-derivatives) are implemented using a higher-order numerical stencil. This was deemed to be necessary to keep the *truncation* error at sufficiently low levels. The temporal and the radial direction related operations are second-order and such a mixed approach yields sufficiently good results.

[3] In recent work [21] we have developed a fifth-order WENO finite-difference scheme with third-order Shu-Osher explicit time-stepping. This new approach yields the same results.

outer boundary is located at null infinity with the same condition. The type of boundary condition does not impact our results. As a concrete example, for $a/M = 0.8$, the inner boundary is located at $\rho = 0.392M$ while the outer one is at $\rho = S = 19.6M$. This range of the compactifying coordinate ρ, implies that the range of Boyer-Lindquist r coordinate stretches from $0.4M$ to infinity. A Penrose diagram that depicts the entire computational domain is shown in Fig. 2. Similarly, for the extremal $a/M = 1.0$ case, the inner boundary is located at $\rho = 0.95M$ while the outer one is at $\rho = S = 19.0M$. In the Schwarzschild cases, we place the inner boundary at $\rho = 0.05M$ while the outer boundary is at $\rho = S = 20.05M$ (these locations are fairly arbitrary). We typically use grid sizes of $8000(\rho) \times 64(\theta)$.

Throughout this work, we choose the initial data for the scalar field to be a Gaussian distribution localized at $\rho = 8.0M$. The angular distribution is an axisymmetric spherical harmonic of multipole ℓ. We include results for both *compact* (a truncated[4] Gaussian with width $0.1M$) and *non-compact* (a wide Gaussian of width $2.0M$) initial data. For the Kerr case, $a/M = 0.8$ except for the extremal case, wherein $a/M = 1.0$, of course.

A. Scalar Fields in Schwarzschild Black Hole Spacetime

We begin with the results for the non-rotating Schwarzschild black hole spacetime case. We present our power-law tails data for the exterior spacetime (horizon, timelike and null infinity) first, followed by the same in the interior region for a number of different multipoles ℓ. We show results for both types of initial data, i.e. with and without compact support.

1. Exterior Spacetime

The expected outcome for the exterior spacetime case is the well-established power-law tail $\tau^{-2\ell-3}$ [3] which is valid at the horizon and timelike infinity, while the expression changes to $\tau^{-\ell-2}$ at null infinity [3]. In these expressions, ℓ is the multipole of the scalar field under consideration, and recall that at the horizon location τ is essentially the null coordinate v.

The data depicted in Table I shows that our approach reproduces these well-established tails and therefore, serves as an excellent check on our methodology. It is worth noting that we tested our implementation for all multipoles up to $\ell = 10$ with excellent agreement with the power-law tail expression [3]. This was found to be the case for both types of initial data (compact and non-compact).

$\ell\backslash\rho$	Horizon	$\rho = 3.0$	Infinity $\mathscr{I}^+$
2	-7	-7	-4
3	-9	-9	-5
4	-11	-11	-6
5	-13	-13	-7
6	-15	-15	-8
8	-19	-19	-10

TABLE I: Asymptotic late-time scalar field tails in exterior Schwarzschild space-time for several multipoles. The power-laws agree precisely with the expected law [3]. The actual numerical values obtained from our computations agree with the values in this table within one-percent.

2. Interior Spacetime

Here we report on some new results in the case of the interior region of the Schwarzschild spacetime. As cautioned before, it is not meaningful to sample the field at a fixed ρ location, because that implies that the detector is on a spacelike worldline. However, nonetheless, if we proceed with that type of data sampling anyhow, it is interesting that the field exhibits late-time power-law decays in the τ coordinate, that generically satisfy the usual law [3]. This can be seen in Figure 3 for a number of different ℓ multipoles. For the high-ℓ cases it is clear that high-precision numerics are necessary, since the field's amplitude falls very rapidly due to the fast decay rate.

For a more physically meaningful detector, we remarked before that a timelike worldline dictates that the detector must continuously fall towards $\rho = 0$, i.e. the radial coordinate must decrease in value monotonically. To understand what type of signal such a detector would record, we plot the snapshots of the field as a function of ρ at different values of τ.

The case of non-compact initial data, is shown in Figures 4, 5 [5]. At early times, we observe many dynamical features as the field evolves through the quasi-normal ringing stage and finally "settles" to more quiescent tail state. In the late-stage tails regime, the field appears to maintain its ρ profile and simply fall in amplitude determined by the usual power-law [3]. However, we observe a number of interesting features in the interior region of the spacetime. In particular, there are ρ "locations" where the field switches sign (this does not happen in the

[4] The truncation is performed using a simple window function of width $10.0M$ centered at $\rho = 8.0M$.

[5] Animations based on the dynamics of the field's radial profile may be found at this URL: `https://www.youtube.com/channel/UCVNLqTQx1O2sbwc-4wsE_Gw`

exterior region). And, in fact, the number of these zero-crossings or "nodes" increases proportionately with the multipole ℓ value. This suggests that a physical detector would observe a finite number of oscillatory cycles in the field *after* crossing into the black hole interior before the detector hits the central black hole singularity. The higher the value of ℓ, the larger the number of cycles the detector would record.

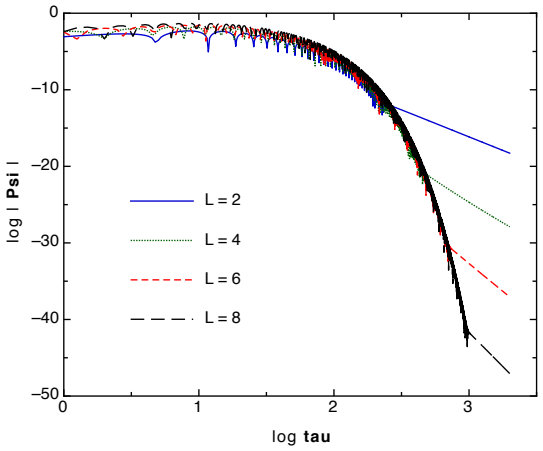

FIG. 3: Late-time scalar field tails for different multipoles ℓ at $\rho = 1$ for the case of Schwarzschild black hole interior. The power-laws agree with the expression $\tau^{-2\ell-3}$.

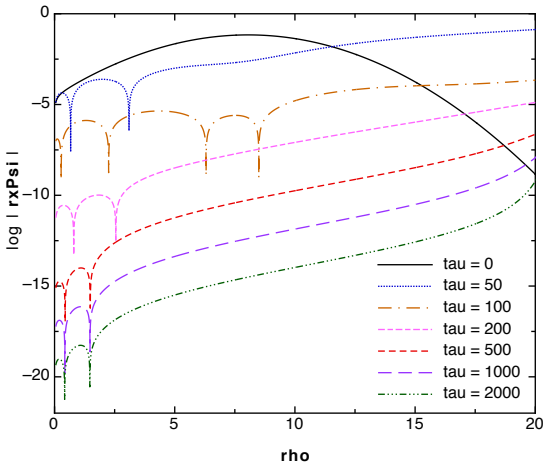

FIG. 4: Late-time scalar field radial ρ profile for multipole $\ell = 2$ for a Schwarzschild black hole. Note that even at late-stages, the field exhibits oscillatory behavior but only in the black hole interior region.

The exact same features also appear in the case of the compact initial data. For that reason, we only document results from one multipole alone, i.e. $\ell = 4$ in Figure 6. The field behaves similar to the non-compact case and the same number and type of zero-crossings are observed in the interior region.

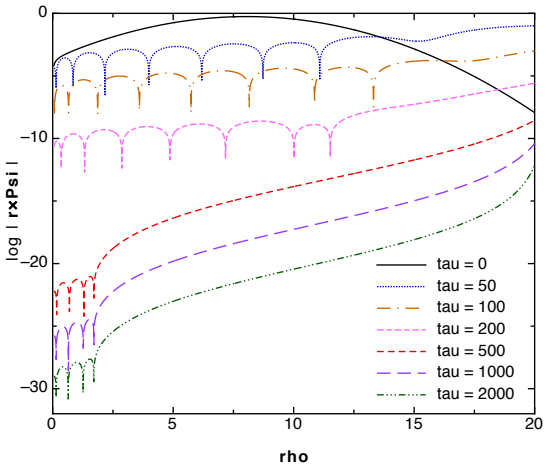

FIG. 5: Late-time scalar field radial ρ profile for multipole $\ell = 4$ for a Schwarzschild black hole. Note that even at late-stages the field exhibits oscillatory behavior but only in the black hole interior region. The number of cycles is proportional to ℓ.

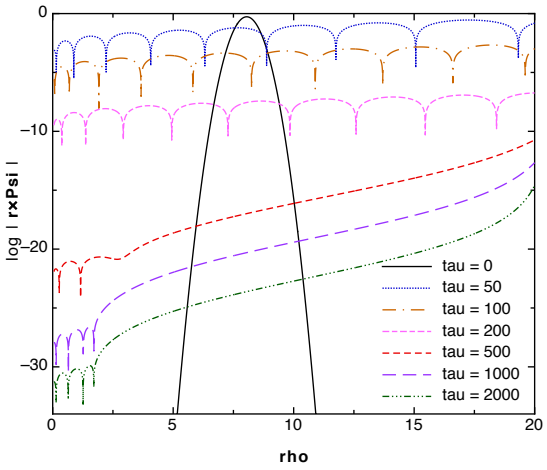

FIG. 6: Late-time scalar field radial ρ profile for multipole $\ell = 4$ for a Schwarzschild black hole. The initial field has compact support. At late-stages the field exhibits oscillatory behavior but only in the black hole interior region. The number of cycles is proportional to ℓ.

At a mathematical level, it is not difficult to uncover the detailed explanation for these oscillations in the interior. Here we derive *analytic* solutions for the location of these late-time nodes found within the Schwarzschild black hole horizon. We begin with the Teukolsky equation for the scalar field Ψ (Eqn. 4) and consider the Schwarzschild case by setting $a = 0$.

Next, we assume separability [24] of the angular, radial and temporal functions such that $\Psi = Y_{\ell m}(\theta, \tilde{\varphi})R(r)T(\tilde{t})$ where the $Y_{\ell m}$ functions are the well-known spherical harmonics. Thus, the radial and temporal part of the

separated differential equation take the form

$$\ell(\ell+1) = -\frac{1}{T}\left((r^2+2Mr)\frac{\partial^2 T}{\partial \tilde{t}^2} - 2M\frac{\partial T}{\partial \tilde{t}}\right) + \frac{1}{R}\left((r^2-2Mr)\frac{\partial^2 R}{\partial r^2} + 2(r-M)\frac{\partial R}{\partial r}\right) + \frac{1}{RT}4Mr\frac{\partial T}{\partial \tilde{t}}\frac{\partial R}{\partial \tilde{r}}. \quad (7)$$

The last term in the equation above prevents clear separability between the radial and temporal dependences. However, motivated by our numerical results, if we let the behavior of the temporal component to be a power law decay, i.e. $T(\tilde{t}) \approx \tilde{t}^{-n}$, then in the limit of $\tilde{t} \to \infty$ the above equation reduces to

$$(r^2-2Mr)\frac{\partial^2 R}{\partial r^2} + 2(r-M)\frac{\partial R}{\partial \tilde{r}} = \ell(\ell+1)R(r). \quad (8)$$

This differential equation takes the form of the well documented Sturm–Liouville problem, with the well-known solutions

$$R(r) = C_1 P_\ell(r/M-1) + C_2 Q_\ell(r/M-1) \quad (9)$$

where P and Q are the Legendre polynomials of the first and second kind respectively. For the solution above to exhibit the correct behavior at the horizon, we must set $C_2 = 0$ and therefore

$$R(r) \propto P_\ell(r/M-1) \quad (10)$$

We note that this solution was also obtained by Ori in Ref. [25]. The roots of $R(r)$ above are in excellent agreement with the location of the nodes we present in Figs. 4, 5 and 6. Thus, we see that the oscillations as observed by an infalling physical detector come from the oscillations in the Legendre polynomials that describe the state of the scalar field on the interior.

B. Scalar Fields in Kerr Black Hole Spacetime

In this subsection we present our results for the rotating Kerr black hole case. Once again we present our power-law tails data for the exterior spacetime (horizon, timelike and null infinity) first, followed by the same in the interior region for a number of different multipoles.

1. *Exterior Spacetime*

Interestingly, only recently has an understanding of the nature of the late-time power-law tails in Kerr spacetime been fully uncovered [22, 26]. The late-time decay rate expressions for the scalar field case are given by τ^n where

$$n = \begin{cases} -(\ell'+\ell+3) & \text{for} \quad \ell' = 0,1 \\ -(\ell'+\ell+1) & \text{otherwise} \end{cases} \quad (11)$$

on the horizon and timelike infinity, and

$$n^{\mathscr{I}^+} = \begin{cases} -\ell' & \text{for} \quad \ell \leq \ell'-2 \\ -(\ell+2) & \text{for} \quad \ell \geq \ell' \end{cases} \quad (12)$$

at null infinity. Here ℓ' refers to the initial field multipole and ℓ is the projected multipole of the full late-time field under consideration. In the Schwarzschild case, these are always the same, i.e. $\ell' = \ell$. However, since Kerr spacetime is not spherically symmetric, a pure ℓ' multipole does not stay pure as it is evolved, i.e. other ℓ multipoles are "excited". In general, even-valued ℓ' modes only excite even ℓ, while the odd-valued ones excite only the odd multipoles. This is because Kerr spacetime still retains a reflection symmetry about the equatorial plane.

The above expressions were obtained by carefully studying the "inter-mode coupling" effects that are present in Kerr space-time due to frame-dragging [26]. Note that these expressions above are only for the axisymmetric multipoles. In our work, we only study the full field throughout, which implies we study the late-time dominant multipole $\ell = 0$ for the even ℓ' case and $\ell = 1$ for the odd case. At late times, clearly these will dominant all other multipoles (they exhibit the slowest decay) and therefore, dominate in the full field. Thus, the above expressions simplify to $\tau^{-\ell'-1}$ for even $\ell' > 0$ and $\tau^{-\ell'-2}$ for odd $\ell' > 1$ at the horizon and timelike infinity. At null infinity they reduce to $\tau^{-\ell'}$ for $\ell' > 1$. In this section, we verify these expressions using our numerical data.

Once again, Table II shows that our approach works correctly and the equations 11, 12 are verified. We tested our implementation for all multipoles up to $\ell' = 8$ with excellent agreement. This is the case for both types of initial data.

$\ell' \backslash \rho$	Horizon	$\rho = 3.0$	Infinity $\mathscr{I}^+$
2	-3	-3	-2
4	-5	-5	-4
6	-7	-7	-6
8	-9	-9	-8

TABLE II: Asymptotic late-time scalar field tails in exterior Kerr space-time for several multipoles. The power-laws agree with equations 11, 12. The actual numerical values obtained from our computations agree with the values in this table within one-percent.

2. *Interior Spacetime*

Our new results in the context of the interior region of the Kerr spacetime are similar to the Schwarzschild case. If we proceed with sampling the field data at a fixed ρ it exhibits late-time power-law decays in the τ coordinate, that generically satisfy the equivalent of the well-known

tails law [3] for Kerr, equation 11. This can be seen in Figures 7, 8 for a number of different ℓ' multipoles.

For a more physically meaningful detector, one that must continuously fall towards $\rho = 0$ once again we observe a finite number of oscillatory cycles due to the formation of zero-crossing nodes in the interior region. This can be seen in Figures 9, 10 that depict the multipole data as a function of ρ for several moments in τ. However, we do not see as many oscillatory cycles as observed in the Schwarzschild case. This is simply because of the dominance of the excited low-ℓ modes at late times that occurs in Kerr spacetime, but not in Schwarzschild. In fact, we observe precisely one zero-crossing in the odd-ℓ' case and none at all in the even-ℓ' case. This is in line with expectations, of course, since $\ell = 1$ is the lowest odd multipole that is excited, while $\ell = 0$ is the lowest one for the even case. We observe the exact same features in the case with compactly supported initial data.

Finally, we also computed the late-stage, power-law tails of a scalar field of different initial multipoles at the Cauchy (inner) horizon of the black hole. Recall that at the horizon locations, the variable τ is essentially the null variable v. Therefore, these results may be compared with Ori's well-known work in a similar context [27]. They are in excellent agreement.

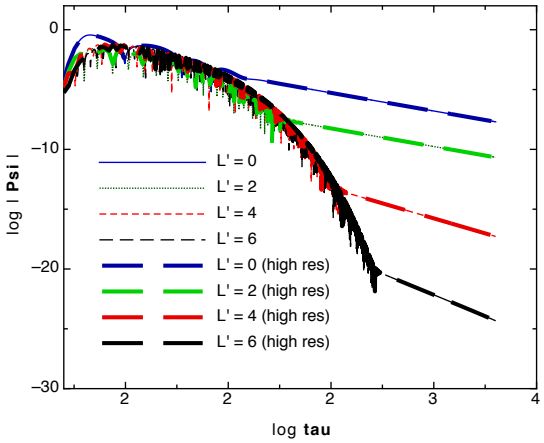

FIG. 7: Late-time scalar field tails for different multipoles ℓ' at $\rho = 1$ of a Kerr black hole interior. The power-laws agree with the equation 11. Data is presented from computations using two different grid sizes $(8000(\rho)\times32(\theta)\times1665972(\tilde{t})$ and $16000(\rho) \times 64(\theta) \times 3331944(\tilde{t}))$, to demonstrate convergence of the numerical results.

C. Scalar Fields in Extremal Kerr Black Hole Spacetime

Recently [13, 14] it has been shown that massless scalar fields in extremal black hole spacetimes exhibit an "asymptotic" instability at the horizon. This arises in the form of an unbounded growth of (sufficiently) high-

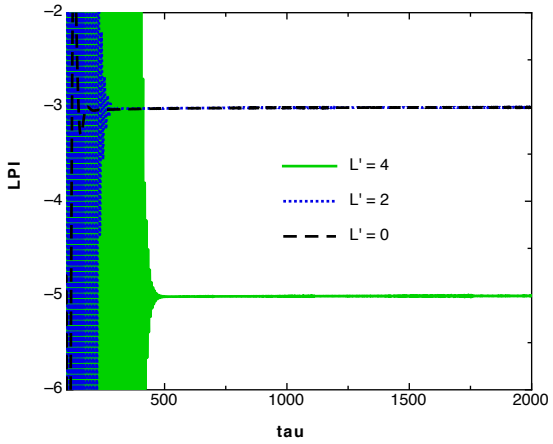

FIG. 8: The local power index (LPI), defined as $n = \tau\dot{\Psi}/\Psi$, for different multipoles ℓ' at $\rho = 1$ of a Kerr black hole interior. The late-time index values agree with the equation 11.

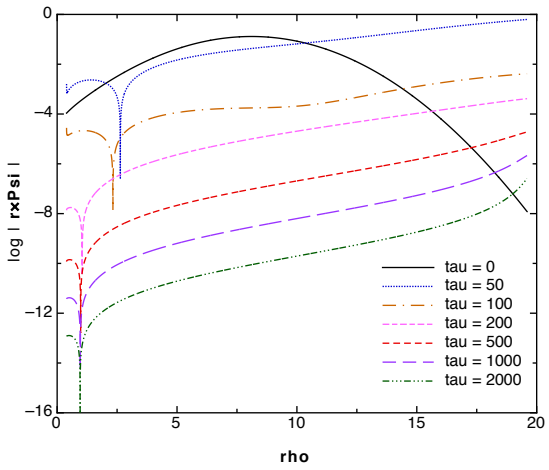

FIG. 9: Late-time scalar field radial ρ profile for multipole $\ell' = 1$ for a Kerr black hole. Note that even at late-stages the field exhibits oscillatory behavior but only in the black hole interior region.

order transverse derivatives of the field. Heuristically, the origin of this instability is in the fact that the power-law tail's decay rate at the horizon is slower than at a "nearby" location on the exterior. This *only* occurs in the case of an extremal hole (note that our results in the previous section on non-extremal Kerr consistently yielded the exact same tail on the horizon as the timelike infinity case). The different decay rate at the horizon results in an unbounded growth in high-enough transverse derivatives. More precisely this instability can be seen as arising from a singular branch-point in the frequency-domain Green function [14]. Our numerical results in the context of extremal Kerr black holes are able to show strong indications of the development of such an instability.

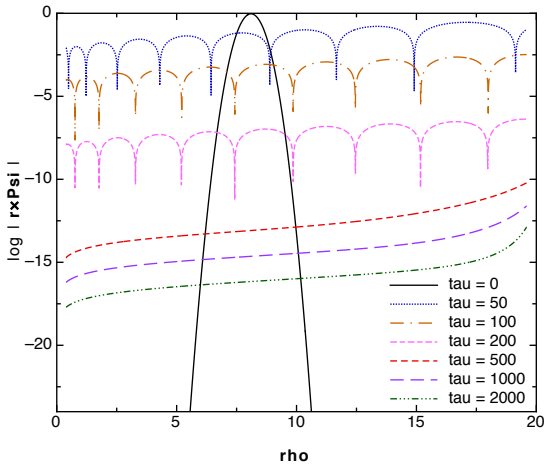

FIG. 10: Late-time scalar field radial ρ profile for multipole $\ell' = 4$ for a Kerr black hole. There are no oscillations at late times because of the dominance of the $\ell = 0$ multipole.

In Figure 11 we show the late-time tails for the extremal Kerr case for a sample multipole with compact initial data – it is clear that the horizon decay rates are slower (they actually match the null infinity rates!) than the timelike infinity cases for the same multipole.

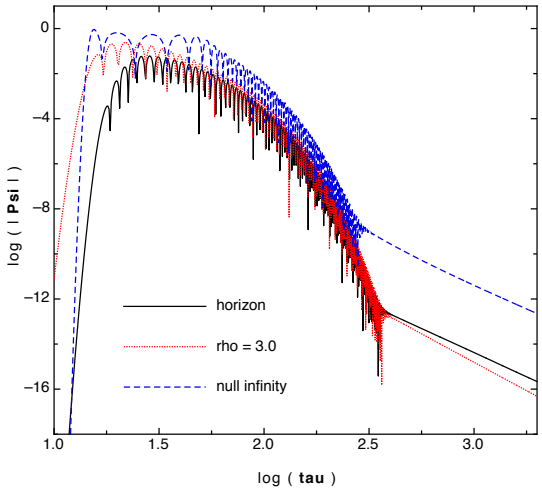

FIG. 11: Late-time scalar field tails for $\ell' = 4$ at different locations (horizon, $\rho = 3.0$ and null infinity) for an extremal Kerr black hole. The horizon decay rate is slower than the $\rho = 3.0$ case, and matches the rate at null infinity.

Moreover, if we study the radial (ρ) profile of the field as it evolves in time, it clearly appears to show the formation of an asymptotic "discontinuity" at the horizon. In Figure 12 we can see that the gradient of the field as it evolves becomes steeper at the horizon, a strong indication of the transverse derivatives becoming unbounded, consistent with the expectations based on recent work [14]. A detailed study on this topic will be presented elsewhere [28].

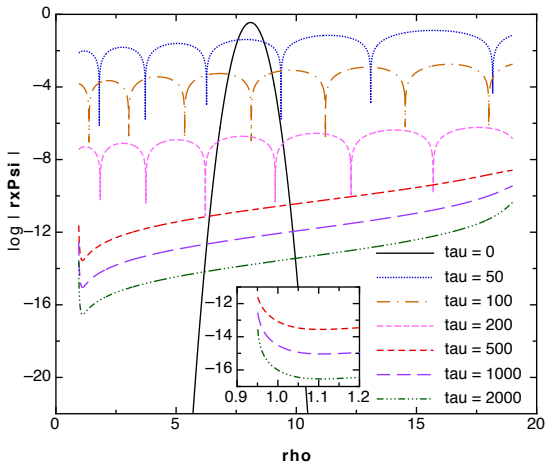

FIG. 12: Late-time scalar field radial ρ profile for multipole $\ell' = 3$ for an extremal Kerr black hole. Note that the field's gradient exhibits unbounded growth at the horizon.

IV. SUMMARY AND CONCLUSIONS

In this work, we performed a detailed study of the late-time tail behavior of scalar fields in black hole exterior and interior spacetimes. Both Schwarzschild and Kerr black holes were considered in this work. We numerically solved the scalar Teukolsky equation in compactified ingoing Kerr coordinates, and performed very long duration computations to obtain the true late-time asymptotic power-law decay behavior. We compared our numerical results with well known results in the research literature in the black hole exterior region (horizon, timelike and null infinity). The new results in this work pertain to the late-time behavior of scalar fields in the black hole interior. We found that an infalling detector would record a finite number of oscillatory cycles in the field before it hits the black hole singularity. The number of these observed cycles depends on the multipole index ℓ of the field and also whether the black hole is Schwarzschild or Kerr. We also found an indication of the formation of an asymptotic instability at the horizon of an extremal Kerr black hole.

In future work, we would like to perform similar investigations of other matter fields, including the electromagnetic and gravitational cases. We also plan to explore the behavior of non-axisymmetric fields in a similar context.

Acknowledgments—We thank Lior Burko and Amos Ori for helpful discussions and for giving us feedback on a previous version of this paper. I.T. and G.K. acknowledges research support from NSF Grants No. PHY-1414440 and No. PHY1606333, and from the U.S. Air Force agreement No. 10-RI-CRADA-09.

[1] B. P. Abbott *et al.* (LIGO and Virgo Scientific Collaborations) Phys. Rev. Lett. **116**, 061102 (2016).

[2] B. P. Abbott *et al.* (LIGO and Virgo Scientific Collaborations) Phys. Rev. Lett. **116**, 241103 (2016).

[3] R. H. Price, Phys. Rev. D **5**, 2419 (1972).

[4] L. Barack and A. Ori, Phys. Rev. Lett. **82**, 4388 (1999); L. Barack, Phys. Rev. D **61**, 024026 (2000).

[5] S. Hod, Phys. Rev. D **58**, 104022 (1998); S. Hod, Phys. Rev. D **60**, 104053 (1999); S. Hod, Phys. Rev. D **61**, 024033 (2000); S. Hod, Phys. Rev. Lett. **84**, 10 (2000); S. Hod, Phys. Rev. D **61**, 064018 (2000).

[6] L.M. Burko and G. Khanna, Class. Quant. Grav. **26**, 015014 (2009); L. M. Burko and G. Khanna, Class. Quant. Grav. **28**, 025012 (2011); I. Racz and G. Z. Toth, Class. Quant. Grav. **28**, 195003 (2011); M. Jasiulek, Class. Quant. Grav. **29**, 015008 (2012); T. Spilhaus and G. Khanna, preprint arXiv:1312.5210; A. Zenginoğlu, G. Khanna and L. M. Burko, Gen. Rel. Grav. **46**, 1672 (2014); L. M. Burko and G. Khanna, Phys. Rev. D **89**, 044037 (2014).

[7] E. Poisson and W. Israel, Phys. Rev. Lett **63**, 1663 (1989); A. Ori, Phys. Rev. Lett. **68**, 2117 (1992).

[8] P. Brady and J. Smith, Phys. Rev. Lett **75**, 1256 (1995); L.M. Burko, Phys. Rev. Lett **79**, 4958 (1997).

[9] L. M. Burko, G. Khanna, A. Zenginoğlu, Phys. Rev. D **93**, 041501(R) (2016)

[10] D. Marolf, A. Ori, Phys. Rev. **D** 86, 124026 (2012); E. Eilon, A. Ori, Phys. Rev. **D** 94, 104060 (2016).

[11] M. Dafermos, Comm. Math. Phys. **332**, 729 (2014); M. Dafermos, I. Rodnianski and Y. Shlapentokh-Rothman, Communications in Mathematical Physics Online first (2016); A. Franzen, Communications in Mathematical Physics **343**, 601 (2014); P. Hintz, preprint arXiv:1512.08003; J. Luk and S.-J. Oh, preprint arXiv:1501.04598 (2015); J. Luk and S.-J. Oh, Journal of Functional Analysis **271**(7), 1948 (2016); D. Philipp, V. Perlick, preprint arXiv:1503.08101.

[12] A. Ori, Phys. Rev. Lett. **83**, 5423 (1999).

[13] S. Aretakis, Class. Quantum Grav. **30** 095010 (2013).

[14] M. Casals, S. E. Gralla, P. Zimmerman, Phys. Rev. D **94**, 064003 (2016).

[15] S. Teukolsky, Astrophys. J. **185** 635 (1973).

[16] C. Misner, K. Thorne, J. Wheeler, *Gravitation*, W. H. Freeman, San Francisco (1973).

[17] M. Campanelli *et al*, Class. Quantum Grav. **18**, 1543 (2001).

[18] A. Zenginoğlu, Class. Quant. Grav. **25**, 145002 (2008); A. Zenginoğlu, Class. Quant. Grav. **25**, 175013 (2008); A. Zenginoğlu, Class. Quant. Grav. **25**, 195025 (2008); A. Zenginoğlu, D. Nunez, S. Husa, Class. Quant. Grav. **26**, 035009 (2009); A. Zenginoğlu, M. Tiglio, Phys. Rev. D **80**, 024044 (2009); A. Zenginoğlu, Class. Quant. Grav. **27**, 045015 (2010); A. Zenginoğlu, J. Comput. Phys. **230**, 2286 (2011); A. Zenginoğlu, Phys. Rev. D **83**, 127502 (2011).

[19] A. Zenginoğlu and G. Khanna, Phys. Rev. X **1**, 021017 (2011). Note that a different approach towards compactification was used therein – a hyperboloidal compactified *layer* was attached to the outer part of a Boyer-Lindquist coordinates based computational grid.

[20] E. Harms, S. Bernuzzi, A. Nagar, and A. Zenginoğlu, Class. Quantum Grav. **31**, 245004 (2014).

[21] Z. Grant, L. Isherwood, S. Gottlieb and G. Khanna, in progress.

[22] A. Zenginoğlu, G. Khanna and L. M. Burko, Gen. Rel. Grav. **46**, 1672 (2014).

[23] G. Khanna, J. Sci. Comput. **56**, 366 (2013).

[24] R. H. Price, unpublished Ph.D. thesis, California Institute of Technology (1971).

[25] A. Ori, Phys. Rev. D **57**, 2621 (1998).

[26] L. M. Burko, G. Khanna, Phys. Rev. D **89**, 044037 (2014).

[27] A. Ori, Phys. Rev. D **58**, 084016 (1998).

[28] L. Burko, G. Khanna, I. Thuestad, *in preparation.*